Plasma shut-down with fast impurity puff on ASDEX Upgrade.

G. Pautasso, T. Pütterich, C.J. Fuchs, O. Gruber, C.F. Maggi, M. Maraschek, V. Rohde, C. Wittmann, E. Wolfrum, P. Cierpka, M. Beck and the ASDEX Upgrade Team

Max-Planck-Institut für Plasmaphysik, EURATOM Association, D-85748 Garching, Germany
e-mail: gabriella.pautasso@ipp.mpg.de

Abstract
The massive injection of impurity gas into a plasma has been proved to reduce forces and localized thermal loads caused by disruptions in tokamaks. This mitigation system is routinely used in ASDEX Upgrade to shut down plasmas with a locked mode. The plasma response to impurity injection and the mechanism of reduction of the mechanical forces is discussed in the paper.

1. Introduction

Plasma disruptions have three major negative effects on a tokamak. They cause: (1) localized deposition of thermal energy on the plasma facing components, (2) generation and consequent deposition of runaway electrons (RE) in the torus and (3) large mechanical forces on the electrically conducting structures. Nevertheless the magnitude of these effects can be significantly reduced by the injection of impurity gas before the thermal quench occurs. Therefore experiments on disruption mitigation are carried out nowadays on all large tokamaks to investigate the influence of the injected impurities on the development of the disruption. The kind of gas, the rate of injection and the injected quantities differ considerably according to the type of gas injection system available, the volume of the vessel and the specific problems affecting the machine after disruption. In this framework, ASDEX Upgrade (AUG) has been conducting experiments for years [1] – [3] and is routinely employing the fast injection of neon for plasma shut-down. The injection is usually triggered by the locked mode signal and leads to the onset of a mitigated disruption within a few milliseconds.
This paper describes the phenomenology of mitigation (Section 2), the experimental conditions in AUG (Sec. 3), the plasma response to the injection of impurities, discusses the understanding of the observed phenomena (Sec. 4) and outlines the plans for the further development of the AUG mitigation system (Sec. 5). The modelling of the complex phenomena following impurity-plasma interaction and the requirements for the application of mitigation techniques in ITER are not discussed in the present paper.

2. Working hypothesis

The injection of a massive impurity gas into a disruptive plasma influences the disruption effects described above since it increases the plasma density and cools the plasma by dilution and radiation before the thermal quench occurs. The optimal disruption mitigation requires that all three deleterious effects of disruptions are reduced below acceptable engineering margins.
In order to reduce the **localized heat deposition** during the thermal quench of the disruption, the injected impurity gas must store (ionization energy) and radiate most of the thermal energy of the plasma before magnetic instabilities can cause the thermal quench. In order to do this, the gas must
1) penetrate as neutral into the plasma - Note that low Z atoms have a larger mean free path -;
2) penetrate fast, i.e. before the thermal quench sets in - Note that low Z, i.e. atomic number, impurities have a faster sound speed: $v_s = \sqrt{kp/\rho}$ (k is the adiabatic constant, p and ρ are the pressure and the density of the gas) -;
3) radiate as much as possible. The specific radiation efficiency f_I, and therefore the radiated power $P_{rad} = f_I n_e n_I$, increases from low to high Z (n_e and n_I indicate the density of electron and impurities respectively).

The suppression of the **RE generation** requires a slow current quench for the reduction of the toroidal electric field below the critical electric field, $E_c \propto n_e/T_e$, and the increase of this threshold through the density.
The reduction of the **forces** follows the reduction of the induced toroidal, poloidal and eddy currents in the structure of the plasma. Depending on the vertical stability characteristics of the plasma, the methods of impurity injection can follow two different strategies.
1) In tokamaks with vertically stable plasmas, the largest mechanical forces are eddy currents caused by the plasma current quench. In this case the current quench should develop slowly. This contributes to the avoidance of the RE. Low-Z impurities are suitable for injection in this case: they penetrate further into the plasma, increase the density and therefore E_c. The mitigation of the thermal load during thermal quench in this case is uncertain.
2) In vertically unstable plasmas instead, the toroidal and poloidal (halo) currents induced in the mechanical structures of the machine must be reduced. The toroidal current in the passive stabilizing loop (PSL) of AUG is induced by the mutual inductance between plasma and loop. The PSL is a massive saddle coil, suspended inside of the vessel, with the function of slowing down the n=0 plasma vertical motion on the time scale of 600 ms and allowing the vertical control by the feedback system. The halo current is mostly induced by the shrinking of the plasma cross section, can reach 30-40 % of the plasma current and contributes significantly to the overall vertical force balance. These currents generate a stabilizing vertical force which counteracts the destabilizing vertical force ($F_{z,dest}$), exerted by the quadrupole magnetic field, which elongates the plasma.

$$F_{z,dest} = 2\pi R_0 I_p \frac{\partial B_r}{\partial z}_{|z_0} (z - z_0) \qquad (1)$$

We can anticipate that, after massive injection of high Z impurity, we observe a plasma current quench, which is anticipated and accelerated at lower values of $(z - z_0)$. The suppression of the RE in the mitigation scheme (2) becomes more uncertain because of the smaller increase of the density following high Z impurity injection.
A further requirement to any mitigation method is the low contamination of subsequent plasma discharges. In fact it is unacceptable to use a type, a quantity of gas or a frequency of injection which significantly contributes to the Z_{eff} of the following discharge.
The type and quantity of gas injected depends on a trade-off among the above requirements and therefore on the specific machine and disruption. While presenting the experimental measurements on AUG, we will discuss to which extent they support the requirements just outlined in this paragraph.

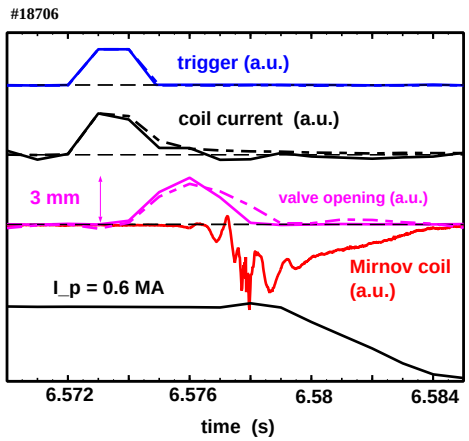

FIG. 1: Temporal sequence of trigger, solenoid current, opening of the valve shutter and onset of the disruption, seen in the Mirnov coils and plasma current.

3. Experimental layout

The impurity gas is injected into the plasma with two electromagnetic valves, originally built by Dr. Sergej Egorov at the Technical University in St. Petersburg, and modified in the IPP Laboratories. The current in the solenoid of the valve is generated by an array of capacitors charged at voltages of 200-300 V. The valves have an opening and closing time of 2 ms and remain open for 4-5 ms. The movement of the valve shutter is monitored by a photosensor, the signal of which is shown in Fig. 1.

The valves have been mostly operating with neon gas up to 5 bar and have been typically injecting 180 mbarl (4.5 10^{21} atoms) of gas. Dedicated experiments have been carried out with 10 and 15 bar. The valves are situated in a large port in sector 13 (AUG consists of 16 sectors) of the tokamak, in the mid-plane, on the low field side and 1.5 m away from the plasma edge. The gas expands firstly into a guiding tube, then in the port and finally into the vessel.
A pressure gauge mounted at the valve records the gas pressure in the valve before and after the gas puff. During the opening time of 4-5 ms, the valve releases 50-70 % of the gas content into the vessel. This quantity is in agreement with the theoretical prediction of the one-dimensional ideal sonic flow of a gas through a nozzle.

4. Measurements of plasma parameters

The plasma measurements discussed in this section pertain to lower or upper X-point plasmas in the shot range 18600 - 21500, in flat-top, with a vertical elongation larger than 1.5, which underwent a disruption with or without neon puff. Since AUG has an elongated and therefore potentially vertically unstable plasma, most of the mitigation experiments were carried out with injection of neon. Neon was chosen instead of helium or argon on the basis of the results of older experiments [1].
The injection of impurity gas was mostly triggered by the locked mode detection system. A few healthy discharges were intentionally shut down by a preprogrammed impurity gas injection. Two saddle coils mounted in the vessel allow the detection of a locked mode. In the shot range analyzed here, 107 discharges suffered a disruption in flat-top followed by a vertical displacement (VD). In 83 of them the mitigation system was active. In 25 of the 107 disruptions the locked mode trigger would have been or was too late for mitigation purposes. The success rate of the locked mode trigger is comparable to the one of a neural network [2] tested a few years ago on AUG.

4.1. Time delay between trigger and start of current quench.

The current quench after impurity injection can begin with the typical current hump, indicating a fast redistribution of the current profile or with the current rolling over towards its decay without any hump. The majority of the induced thermal quenches has a reduced (with respect to natural disruptions) or no current hump, which is a feature influencing the VD dynamics (see Section 4.8). It is not clear what determines one behaviour or the other one. For the discharges with a clear current hump we define a delay time Δt_{delay}. This time interval is the sum of the gas flying time (Δt_{fly}), from the valve opening to the plasma edge (of approx 2 ms), and of the cooling time (Δt_{cool}).

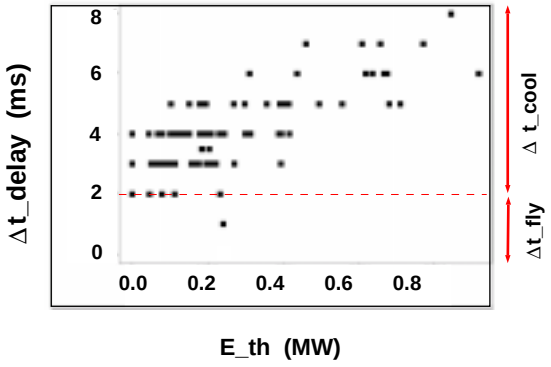

FIG. 2: Time interval between trigger and thermal quench as function of the plasma thermal energy.

Δt_{cool} is observed to vary from zero to 6 ms mostly depending on the thermal energy of the target plasma (see Fig. 2).
A dependence of Δt_{cool} on q_{95} is not clearly found in the data, contrary to recent DIII-D results [5] and expectation. Surprisingly, the quench time does not seem to depend significantly on the flux of the incoming particles either (that is on the pressure of the gas in the valve and on the number of valves used) as we would expect from the energy balance equation:

$$E_{th}(t_0) - E_{th}(t_{th.qu.}) \simeq \Delta t_{cool} P_{rad} \propto \Delta t_{cool} Vol\, Z_I\, n_I^2 \qquad (2)$$

This implies that the impurity density in the plasma during the cooling phase cannot be arbitrarily increased by gas puffing, at least in the range of gas pressure investigated up to now.

4.2. Electron density.

AUG is equipped with several diagnostics for the measurement of the electron density. Among them, the CO2 interferometer and the lithium beam diagnostic can record the fast changes of the electron density following the gas puff.

The CO2 interferometer located in sector 11 measures the line integrated electron density along two vertical cords through the plasma core and plasma periphery on the high field side. This interferometer is not subject to fringe jumps during the disruption and provides believable measurements during the whole thermal and current quench.

A database of line integrated densities before ($N_{e(before)}$) and after ($N_{e(after)}$) the disruption reveals a large range of changes of the density during the thermal quench. Both decrease and increase of the density are observed in natural disruptions. Figures 3 (a) and (b) show scatter plots of $N_{e(after)}$ versus $N_{e(before)}$ as seen by the channel V-1 and V-2 respectively. $N_{e(before)}$ is the line integrated density averaged in the time interval $[(t_{th.qu.} - 20\,ms) - (t_{th.qu.} - 10\,ms)]$. $N_{e(after)}$ is averaged in $[t_{th.qu.} - (t_{th.qu.} + 5\,ms)]$. $N_{e(after)} / N_{e(before)}$ seen by channel V-1 has a large standard deviation and is in average 1.5 and 1.8, respectively for unmitigated and mitigated disruptions. $N_{e(after)} / N_{e(before)}$ seen by channel V-2 is on average of the order of 10, independent of mitigation.

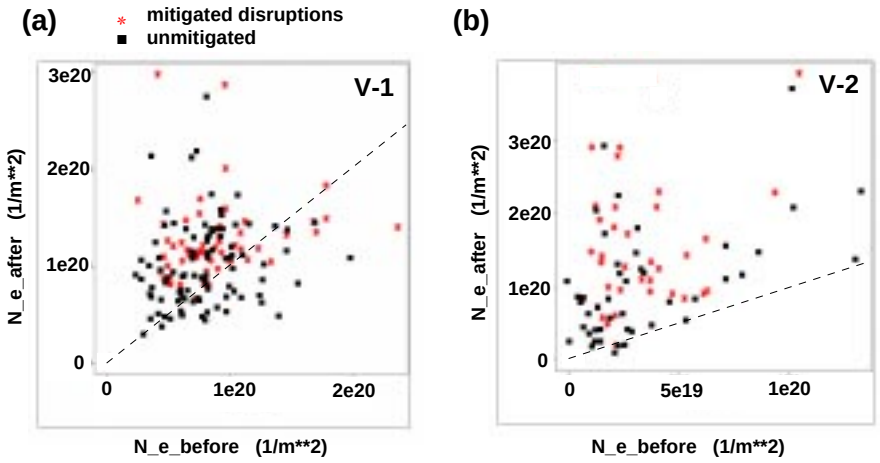

FIG. 3: Scatter plot of the line average density after the disruption versus the line average density before disruption seen by (a) channel V-1 and (b) V-2.

We must conclude that the gas puff does not contribute to a significant increase of the bulk plasma density after the thermal quench. The edge density can increase significantly during the thermal quench independently of the gas puff. The location and the mechanism of this increase cannot be investigated further with these integrated density measurements.

The lithium beam diagnostic located in sector 9 views horizontal profiles of the plasma edge 30 cm above the midplane. After the neon puff, it reveals an increase of the electron density in the SOL of 1 order of magnitude within its finest time resolution interval of 1-2 ms. However this diagnostic cannot measure the density profile after the onset of the (natural or induced) thermal quench because the observed LiI emission is dominated by background radiation in this phase.

4.3. Concentration of neon in plasma after fast shut-down.

The concentration of neon (c_{Ne}) in the plasma is routinely measured and analyzed. A comprehensive discussion of the results of the analysis is going to be published elsewhere [4]. c_{Ne} is derived from the intensity of the Lymann-α emission line of hydrogen-like neon. This line is measured several times during a discharge by a scanning Bragg-spectrometer.

Typically, the emission originates from the edge of the confined plasma at $T_e \simeq 900$ eV. The interpretation of the measurement involves assumptions on the plasma transport at the edge,

which affects the fractional abundance of the emitting ionization state. Its relative uncertainty was estimated by comparison with transport simulations using typical transport parameters for AUG. Taking into account the additional error bars affecting the electron profiles and the absolute calibration of the spectrometer, the total uncertainty of the derived c_{Ne} amounts to a factor of 2-3.

The time history of c_{Ne} in the four discharges following 206 fast shut-downs with neon injection is presented in Fig. 4. Helium-glow discharges, always performed after a disruption and occasionally among discharges, are disregarded in this analysis. Large values of c_{Ne}s, in the range of several percent, may be observed during the first two seconds of the discharge following neon injection. c_{Ne}s decreases significantly during the same discharge. Nevertheless a large scatter in c_{Ne} is observed even directly after a fast shut-down with neon. To investigate the origin of the scatter, the dependences of c_{Ne} on the parameters of the mitigated disruption and of the subsequent discharges have been analyzed. It is found that:

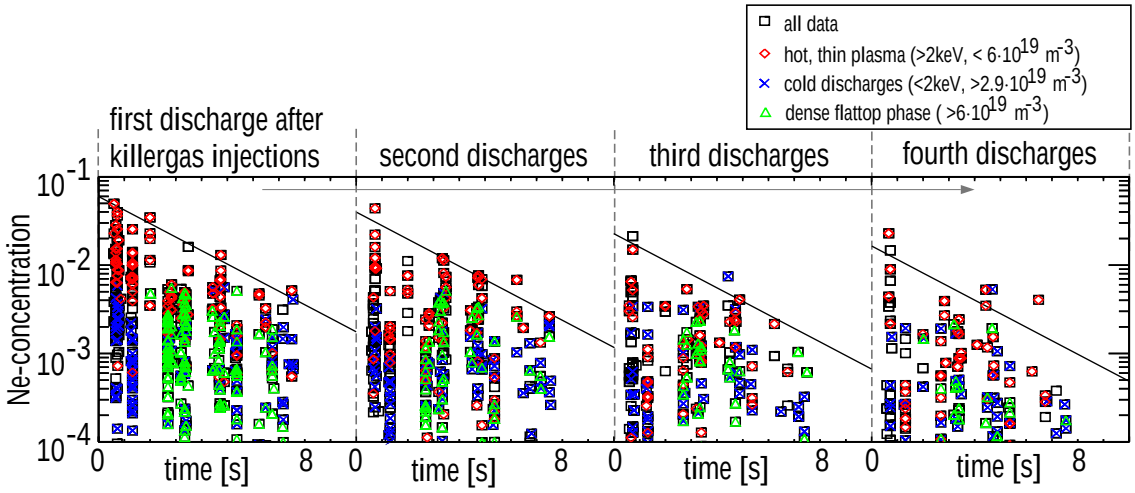

FIG. 4: Neon-concentrations in discharges following a fast shut-down by neon injection. Red diamonds denote measurements from plasmas with $T_e > 2\,keV$ and $N_e < 6 \cdot 10^{19} m^{-3}$, while blue crosses are drawn for plasmas with $T_e < 2\,keV$ and $N_e > 2.9 \cdot 10^{19} m^{-3}$. Green triangles denote flat-top phases with $N_e > 2.9 \cdot 10^{19} m^{-3}$.

(1) If the subsequent discharges are *cold* (i.e. $T_e(0) < 2$ keV and $N_e > 2.9 \cdot 10^{19}\,m^{-3}$, blue in Fig. 4), they exibit a lower neon concentrations. In this type of discharges, larger c_{Ne} are found in the plasma if the neon injection occurred before the thermal quench of the disruption. Also for these discharges, a recent boronization reduces the neon source at the wall.

(2) For *hot and thin* subsequent discharges (i.e. $T_e > 2$ keV and $N_e < 6 \cdot 10^{19}\,m^{-3}$, red in Fig. 4) the distance from a boronization does not significantly influence c_{Ne}. These hot discharges exhibit the highest c_{Ne} found after neon injection, which is of the order of some percent in the first 2 seconds of the discharge.

(3) The difference between the two sets of discharges is most pronounced for the first discharge after a neon injection, while for the following discharges the scatter within each data set extends further towards smaller c_{Ne}. In this case the pumping efficiency (i.e. efficiency in removing the neon from the wall and transporting it to the divertor pumps, which strongly depends on plasma parameters) of the preceding discharges determines how much neon is left at the wall. This leads to the conclusion that a discharge with auxiliary heating during ramp up might be preceded by wall cleaning.

(4) For discharges with $N_e > 6 \cdot 10^{19}\,m^{-3}$ during the flat-top phase (green triangles), c_{Ne}s stays below a few permill, which translate in a small influence of neon on Z_{eff}.

(5) An increase of c_{Ne} from the 2004/2005 to the 2005/2006 campaign is found in the database and it might have different causes. Firstly, the amount of neon injected for mitigation was increased by a factor 2-3. Secondly, changes in the wall condition may have played a role, since helium-glow discharges were applied routinely in the 2004/2005 campaign and avoided in the 2005/2006 one. This was done because the tungsten wall of ASDEX Upgrade had proven to store and release helium very efficiently [6]. Another possible reason for the historical smaller c_{Ne} is that either the helium-glow discharges removed neon from the walls or the walls loaded with helium prevented the storage of neon. This topic will be investigated further in the 2007 campaign.

4.4. Temperature, SXR and MHD activity.

Measurements (ECE) of electron temperature profiles show the effect of the impurity on the plasma. Figure 5 illustrates the time history of several ECE channels. The gas valve is opened at t = 1.310 s in this case. After 2 ms the edge channels record a decrease of the temperature. The whole profile narrows in the following 2 ms without affecting the temperature within the $\rho_\theta < 0.6$ region.

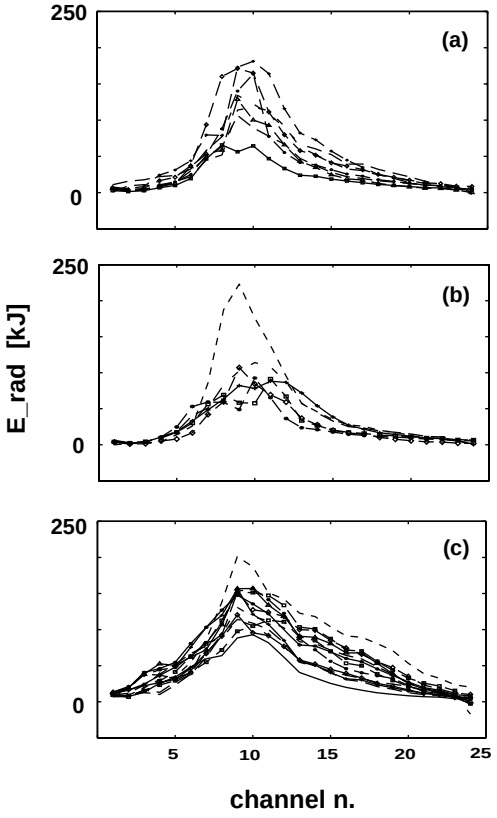

FIG. 5: Profiles of energy radiated in (a) natural disruptions followed by VD, (b) VDEs and (c) disruptions initiated by impurity puff.

Afterwards the whole temperature profile collapses within 0.1 ms as in a natural thermal quench. Data on electron temperature profiles during a gas puff are rare because (1) the ECE measurements are often in cut-off in pre-disruptive plasmas with a large density or go in cut-off after puffing, and (2) the YAG measurements are still too slow to provide a time history of the temperature profile. The SXR diagnostic shows a similar behavior of the line integrated emission.

The massive injection of impurities triggers the onset of large MHD activity. In the case of a neon puff triggered by the locked mode detector, the plasma is not rotating and the structure of the growing fast modes cannot be described with a definable structure or the usual (m,n) numbers. In the few cases of a neon puff in a healthy plasma, the fast growing mode retains the dominant (m,n) structure of the small existing rotating pre-disruption mode (3,1: for example).

4.5. Radiated energy.

The bolometer viewing the plasma chamber vertically from the top of the vessel was used for the comparison of power radiated in disruptions with and without impurity puff. A subset of 21 shots with I_p = 0.9-1.1 MA and lower X point was chosen for this comparison. Figure 6 shows the radiated energy profile of (a) 8 natural disruptions followed by VD, (b) 5 VDEs (vertical displacement events), that is VDs followed by disruptions, and (c) 13 disruptions induced by impurity puff. The radiated energy pertains to the time interval $[(t_{disr} - 3ms) - (t_{disr} + 30ms)]$. The evident differences among the three figures are that VDEs radiate less energy (with the exception of one shot) and the profiles with impurity injection are broader, with more energy seen by the peripheral channels.

The larger amount of radiated plasma energy after mitigation is partly due to the larger energy

of the plasma at the time of mitigation and partly to the effect of the injected impurity.

4.6. Runaway electrons.

Runaway electrons are rare events and appear only in discharges with target density $n_e < 4\,10^{19}$ m^{-3} and $B_t > 2$ T. The process of generation-suppression of RE was not specifically studied in AUG.

4.7. Mechanical loads.

The larger mechanical forces acting on the vessel during natural disruptions are due to larger induced currents in the halo region and in the PSL. The measurements indicate that both type of currents are reduced by a factor of 2-3 by the injection of neon gas.

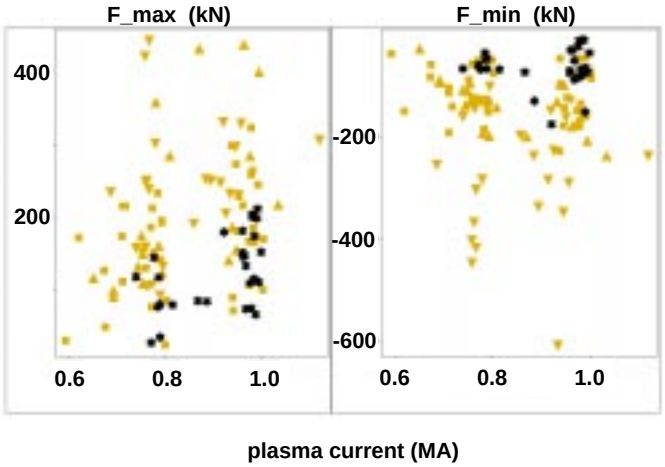

FIG. 6: Maximum and minimum force on vessel versus plasma current. The dark symbols indicate mitigated disruptions

As a consequence, the total vertical mechanical force acting on the vessel and measured by strain gauges at the vessel suspension rods is reduced by a factor of 2-3 with respect to its representative values in unmitigated disruptions (Fig. 7). In addition, a clear correlation between maximum forces on the vessel and maximum vertical excursion of the plasma, as predicted by Eq. (1), is found in the database.
Dedicated experiments with larger gas pressure (15 bar) and gas quantity (factor of 3) show a further reduction of the forces and motivate the use of stronger impurity puffs.
The reduction of mechanical loads in disruptions induced by the impurity gas puff in healthy plasmas is stronger than in plasmas with a locked mode. In the case of healthy plasmas with higher E_{th}, the time interval between trigger and thermal quench may be a few ms longer than in the case of plasmas with a locked mode and a larger impurity density may accumulate at the plasma boundary and enter the plasma during the thermal quench. As a consequence the mitigation experiments with non-disruptive plasmas may lead to overestimating the beneficial effect of impurity injection.

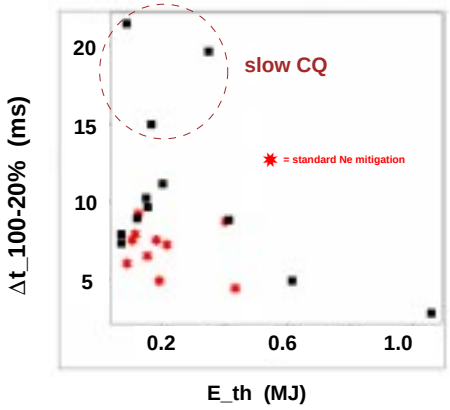

FIG. 7: Current quench (CQ) duration for mitigated and natural disruptions versus thermal energy.

4.8. Rate of current quench and VD dynamics.

The mechanism of reduction of the vertical forces on the vessel can be further investigated by looking at the rate of current quench of mitigated and unmitigated disruptions. Figure 8 shows $\Delta t_{100-20\%}$ as function of the plasma thermal energy for shots with I_p = 0.9-1 MA. $\Delta t_{100-20\%}$ is the time interval in which the toroidal plasma current decays from 100 (at the thermal quench) to 20 % of its value. With the exception of three data points pertaining to disruptions with a slow current quench (the plasma current does not decay significantly while undergoing the VD after the thermal quench), the range of variation

of $\Delta t_{100-20\%}$ does not differ substantially between mitigated and unmitigated current quenches. Moreover, disruptions of hot plasmas may give rise to current quenches faster than the ones induced by mitigation. The current quench time in VDEs (not shown in the picture) is also very fast.

A further analysis of the experimental data reveals a difference in the dynamics of the vertical displacement which is common to a large percentage of the analyzed disruptions. The reduction of the current before the thermal quench and the reduced current hump influence the dynamics of the plasma VD. This behavior is understood in terms of a different interaction between the toroidal currents induced on the machine (vessel and PSL) and the plasma. The result is a smaller vertical plasma excursion at large current which has a beneficial effect on the vertical forces, as predicted by Eq.s (2) and (4).

5. Conclusions

Mitigation of disruption loads by means of impurity injection is routinely used in ASDEX Upgrade to protect the machine. The number of impurity atoms injected during the fast shut-down amounts to 50-100 % of the plasma inventory. Nevertheless most of the impurity atoms do not penetrate into the plasma before the thermal quench and build up a cooling mantel at the SOL. The resulting disruption is similar to a density-radiation limit disruption with fast narrowing of the temperature profile, peaking of the plasma current (increase of the internal inductance observed) and onset of MHD modes leading to disruption.

The neon content in shots following a fast plasma shut-down may accumulate and influence the performance of the following discharges. Therefore the injection of impurities should be limited to the dangerous disruptions and its efficiency optimized.

The mitigation of the mechanical forces after impurity injection is robust and largely documented. The impurities do not accelerate significant the current quench but modifies the dynamics of the vertical displacement. Dedicated experiments with larger (factor of 3) gas pressure and gas quantity show a further reduction of the forces and motivates the use of stronger impurity puffs. The effect of impurity injection on the thermal loads onto plasma facing components requires a dedicated analysis, which is still underway.

A new valve is being developed further to enable operation with a reservoir pressure up to 50 bars. The modified valve will allow us to investigate further the reduction of forces and heat loads as function of the injected number of atoms and gas pressure. Mixtures of hydrogen isotopes and middle-high Z gases, which seem to reconcile deep and fast penetration, high radiation cooling and low residual plasma contamination, will be investigated in the coming future.

References

[1] G. Pautasso et al., *Mitigation of disruptions with fast impurity puff on ASDEX Upgrade,* EPS 2002, Montreux (Switzerland)

[2] G. Pautasso et al., Fusion Science and Technology **44** (2003) 716

[3] G. Pautasso et al., *Plasma shut-down with fast impurity puff on ASDEX Upgrade,* EPS 2005, Tarragona (Spain)

[4] T. Püetterich et al., to be published.

[5] E.M. Hollmann et al., *DIII-D studies of massive gas injection fast shut-downs for disruption mitigation,* EPS 2006, Rome (Italy)

[6] V. Rohde et al., *Wall conditioning in ASDEX Upgrade,* PSI-17, May 2006, Hefei (China)